
EFFICIENT EXPLORATION OF HIGH-T_c SUPERCONDUCTORS BY A GRADIENT-BASED COMPOSITION DESIGN

Akihiro Fujii

Department of Materials Engineering
University of Tokyo
akihiro.fujii@cello.t.u-tokyo.ac.jp

Koji Shimizu

Department of Materials Engineering
University of Tokyo
shimizu@cello.t.u-tokyo.ac.jp

Satoshi Watanabe

Department of Materials Engineering
University of Tokyo
watanabe@cello.t.u-tokyo.ac.jp

ABSTRACT

We propose a material design method via gradient-based optimization on compositions, overcoming the limitations of traditional methods: exhaustive database searches and conditional generation models. It optimizes inputs via backpropagation, aligning the model's output closely with the target property and facilitating the discovery of unlisted materials and precise property determination. Our method is also capable of adaptive optimization under new conditions without retraining. Applying to exploring high-T_c superconductors, we identified potential compositions beyond existing databases and discovered new hydrogen superconductors via conditional optimization. This method is versatile and significantly advances material design by enabling efficient, extensive searches and adaptability to new constraints.

Keywords Deep Learning · Artificial Electromagnetic Materials · Inverse Problem

Material design at the atomic scale has become increasingly important in industry and fundamental research. One of the most interesting fields is the design of high critical temperature superconductors. Superconductors, having no electrical resistance, can significantly enhance the efficiency and performance of the power infrastructure[34]. Discovering high-temperature superconductors that exhibit superconductivity at higher temperatures can reduce cooling costs, thereby accelerating industrial application.

Recently, machine learning has become an essential tool for materials design. The most popular methods in material design at the atomic scale, including the design of high-temperature superconductors, are two: the exhaustive database search (EDS)[3, 4, 5, 6] where trained model searches for materials with predicting materials in databases; conditional generation models[26, 27, 28, 29, 30, 31] employing conditional variational autoencoders (cVAEs)[23], conditional generative adversarial networks (cGANs)[24], or diffusion models[25]. However, they have drawbacks. The EDS

often fails to discover new materials absent from existing databases. Though conditional generation models can generate new materials beyond existing databases, the properties of generated materials are uncertain, requiring validation through other methods. Additionally, introducing conditions beyond the target property necessitates retraining.

The gradient-based approach, where the gradient information of a deep learning model is utilized to optimize inputs through backpropagation, directly optimizes the design parameters of artificial electromagnetic materials (AEMs)[1, 2]. This method may solve the challenges in atomic-scale material design, but a differentiable representation of atomic compositions is indispensable for applying this method to atomic-scale material design because of the use of backpropagation.

In this study, we propose Gradient Driven Material Composition Design (GDMCD), enhancing the gradient-based method for atomic-scale material design through the use of differentiable composition representations[3]. The GDMCD optimizes inputs \hat{x} , differentiable compositions,

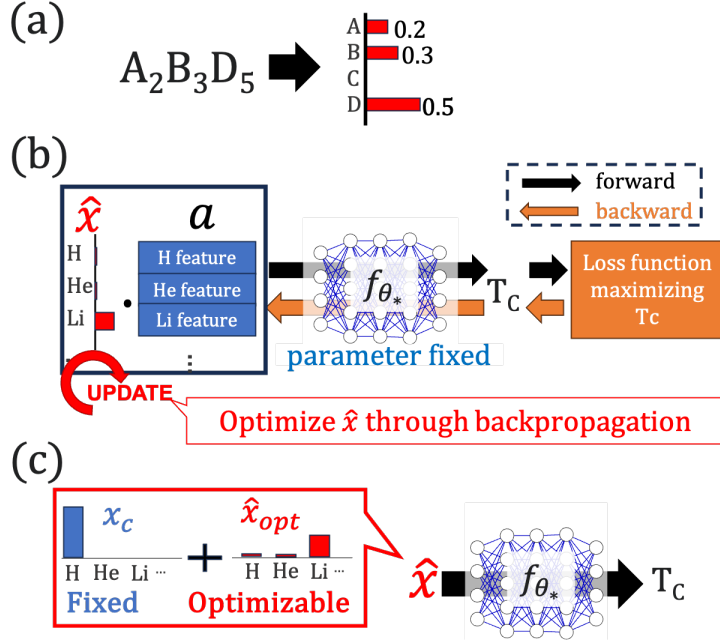


Figure 1: Overview of GDMCD. (a) Compositions are converted into normalized atomic distributions. (b) The optimization of atomic distribution, \hat{x}_t , aims to get compositions with high-Tc using the pretrained model f_{θ_*} , and atomic features a , by minimizing the distance through backpropagation. The black dot denotes matrix multiplication. (c) Adaptive conditional optimization by dividing the inputs into fixed and optimizable parts.

with gradient information to minimize the loss between the desired property and the output from the pretrained model f_{θ_*} (Fig. 1). The GDMCD facilitates exploration beyond existing databases, enabling the search for materials with non-integer compositional values that arise from subtle adjustments, such as doping or elemental substitutions. It allows for immediate and precise determination of the proposed material’s properties using pretrained models. It also supports adaptive conditional searches without the need for retraining, for instance, by fixing parts of the inputs.

We applied GDMCD to search for new high critical temperature (high-Tc) superconductors. As a result, we maximized the Tc of materials from the SuperCon[13] dataset by fine-tuning compositions (e.g. $Ba_{0.9}Y_3Pr_2Cu_{0.1}$ (Tc=85.1 K) \rightarrow $Ba_5Y_3Pr_4Cu_9$ (Tc=129.3 K) and $CaSrBi$ (Tc=109.0 K) \rightarrow $Ca_{3.599}Sr_{9.401}Bi_6$ (Tc=136.9 K)). Additionally, we identified candidates with element combinations not present in the dataset. Furthermore, by employing conditional optimization with the constraint that hydrogen must be included, we discovered hydride superconductor candidates that are similar to recently discovered ones but not included in the dataset (e.g., Y_3H_{10} (Tc=17.7 K)).

The GDMCD is comprised of three stages(Fig. 2). In the first stage, we train a model f with the parameter θ to predict Tc (y) from the composition x and the atomic features a . We discuss x and a in detail later.

$$f : x \rightarrow y, \quad (1)$$

$$\theta_* = \operatorname{argmin}_{\theta} \mathbb{E}_{x,y \sim D_{train}} [L_{train}(y, f_{\theta}(x; a))]. \quad (2)$$

Here, D_{train} represents the training dataset, which consists of pairs of material compositions and their corresponding critical temperatures. The loss function L_{train} measures the discrepancy between the predicted and actual temperatures. At the same time, \mathbb{E} denotes the expectation, calculating the average loss over all samples in the training dataset. After training, we over the predictive model with optimized parameters, f_{θ_*} .

Second, we fix the parameters of f_{θ_*} and optimize solution candidates \hat{x} via backpropagation to increase the output Tc (y) to achieve y_t :

$$L_{2nd}(y_t, y) = \max(0, y_t - y), \quad (3)$$

$$\hat{x}_{t2} = \operatorname{argmin}_{\hat{x}} L_{2nd}(y_t, f_{\theta_*}(\hat{x}; a)). \quad (4)$$

These two stages are done in the same manner as in the previous methods[1, 2]. In the final stage, we employ a special loss function to adjust the compositions to values that can be converted to integers. The composition ratios in \hat{x}_{t2} obtained in the second stage are continuous values (e.g. $Ca_{0.23}Sr_{0.27}O_{0.50}$). However, in this form, unit cell configuration remains unclear. While a simple rounding

method is conceivable, such rounding may deteriorate the maximized Tc. Therefore, we propose a loss function L_{int}^N to make the compositions integer while preserving Tc. Specifically, by specifying the number of atoms N within the unit cell, L_{int}^N guides the composition ratios x_t^i toward the nearest values set c_n^N that can be converted to integers.

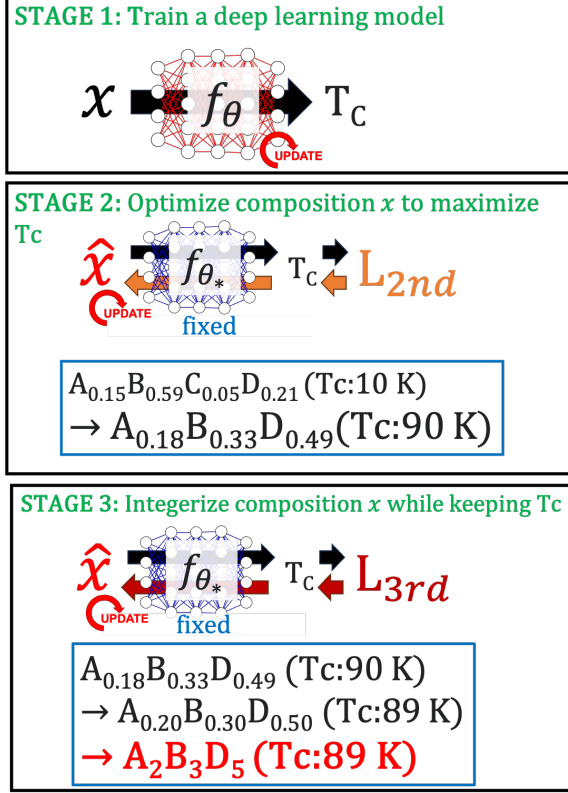


Figure 2: Three stages of GDMCD. At first, we train a deep learning model predicting Tc from composition x . Second, Optimize x to maximize Tc. Finally, we integerize composition \hat{x} while keeping Tc.

$$\{c_n^N\} = \{n/N\}_{n=0,1,\dots,N} \quad \{\hat{x}_t^i\} = \{\hat{x}_t^H, \hat{x}_t^{He}, \hat{x}_t^{Li}, \dots, \hat{x}_t^{Og}\} \quad (5)$$

$$L_{int}^N(\hat{x}) = \sum_{i=1}^{118} \min_n |\hat{x}_t^i - c_n^N| \quad (6)$$

An example for N=4 is illustrated in Fig. 3. The set $\{c_n^4\}$ is $\{0.0, 0.25, 0.5, 0.75, 1.0\}$. As described in the bottom left of Fig. 3, the composition achieving the lowest loss is $Ca_{0.25}Sr_{0.25}O_{0.50}$, resulting in $L_{int}^4 = 0.04$. Multiplying this composition by N yields the integer-based composition $CaSrO_2$. Furthermore, by exempting certain atoms from the loss, we can facilitate element substitution or doping. Atoms a and b are chosen to be exempt

from the loss to minimize $L_{int, ES}^N$, facilitating element substitution (ES).

Example of 4-element unit cell (N=4)

| $\{c_n^4\} = \{$ | Ca _{0.23} | Sr _{0.27} | O _{0.50} |
|------------------|--------------------|--------------------|-------------------|
| 0.00 | 0.23 | 0.27 | 0.50 |
| 0.25 | 0.02 | 0.02 | 0.25 |
| 0.50 | 0.27 | 0.23 | 0.00 |
| 0.75 | 0.52 | 0.48 | 0.25 |
| 1.00 | 0.77 | 0.73 | 0.50 |
| $\}$ | | | |

$$L_{int}^4 = 0.04 \quad L_{int, ES}^4 = 0.0 \text{ (a,b=Ca, Sr)}$$

$$\rightarrow Ca_{0.25}Sr_{0.25}O_{0.5} \quad \rightarrow Ca_{0.23}Sr_{0.27}O_{0.5}$$

$$\rightarrow CaSrO_2 \quad \rightarrow Ca_{0.92}Sr_{1.08}O_2$$

Figure 3: L_{int}^N and $L_{int, ES}^N$ for N=4. The loss function L_{int}^N is defined as the sum of the minimum absolute differences from c_n^4 , allowing for conversion to integers. Conversely, $L_{int, ES}^N$ permits fractional compositions for two specifically selected elements, a and b.

$$L_{int, ES}^N(\hat{x}) = \min_{a,b} \left[\sum_{i \neq a,b} \min_n |\hat{x}_t^i - c_n^N| \right] \quad (7)$$

An example is presented in the bottom right of Fig. 3. In this case, the loss is minimized by exempting atoms Ca and Sr from the loss, resulting in $L_{int, ES}^N = 0$. In practice, as the suitable number of atoms N for the unit cell is unknown, we devise a loss function to select optimal N with the minimal loss from $\{N\}$ ($N \in \{N\}$).

$$L_{integer, \{N\}}(\hat{x}) = \min_{N \in \{N\}} L_{int}^N(\hat{x}) \quad (8)$$

$$L_{3rd}(\hat{x}, y_t, y) = L_{2nd}(y_t, y) + \alpha L_{integer, \{N\}}(\hat{x}) \quad (9)$$

$$\hat{x}_{t3} = \operatorname{argmin}_{\hat{x}_{t2}} L_{3rd}(\hat{x}_{t2}, y_t, f_{\theta_*}(\hat{x}_{t2}; a)) \quad (10)$$

Here, α is a hyperparameter. It is noteworthy that although L_{int}^N is employed in Eq. 10, $L_{int, ES}^N$ could be used alternatively as well.

To utilize the gradient-based methods[1, 2] for atomic-scale material design, we propose making inputs differentiable by representing compositions as distributions of atoms. Specifically, the input data involves multiplying the normalized distribution vector x (Fig. 1 (a)) by the atomic feature tensor a (Fig. 1(b)). Here, the atomic distribution vector x represents the presence ratio of 118 types of atoms (from H to Og) and is normalized to sum to one.

$$x \in \mathbb{R}^{118}, \quad 0 \leq x^i \leq 1 \quad \forall i \in \{1, \dots, 118\} \quad (11)$$

$$\sum_{i=1}^{118} x^i = 1 \quad (12)$$

Note that the normalization condition (Eq. 12) is applied during the optimization of both Eq. 4 and Eq. 10.

For atomic features a , we utilized a representation of s, p, d, and f electron orbitals embedded in the periodic table[3]. See supplementary material S1 for details. Note that we can employ other atomic features instead if they are differentiable. Additionally, GDMCD allows adaptive conditioning of the atomic distribution \hat{x} . Specifically, we achieve this by decomposing the atomic distribution \hat{x} into optimizable and non-optimizable parts (Fig. 1(c)).

$$\hat{x} = \hat{x}_{opt} + x_c \quad s.t. \quad \sum_{i=1}^{118} \hat{x}^i = 1, \quad 0 \leq \hat{x}^i \leq 1 \quad (13)$$

Here, \hat{x}_{opt} is a learnable parameter, and x_c is a fixed conditional vector that cannot be optimized. GDMCD enables adaptive conditional optimization under various conditions by changing x_c .

Next, we explain the optimization results of GDMCD. First, we trained a deep learning model f_{θ_s} to predict the critical temperature (Tc) from compositions, utilizing the SuperCon dataset as the source of superconductor data. Konno et al.[3] pointed out that training only on the SuperCon dataset increases false positives (i.e., mistakenly predicting non-superconductors as superconductors), so we added the Crystallography Open Database (COD)[14, 15, 16, 17, 18, 19, 20, 21, 22] as a dataset of non-superconductors to training data (see supplementary materials S2, S3 in details). We train the ResNet18[11] regression model using Adam optimizer[10], batch size 265, and learning rate 0.01. Given $T_c \geq 0$, we employed the Rectified Linear Unit (ReLU) as the activation function at the output layer.

Since previous methods[5, 4, 9, 8, 7] were evaluated only on SuperCon data, we first evaluated our model solely on the SuperCon dataset (Table 1). Note that it is not a direct comparison due to differences in dataset dividing. Our model was the only one trained on both SuperCon and COD datasets. Because the COD dataset lacks superconductors, its inclusion in the training data might not improve the accuracy of superconductor predictions and could potentially introduce noise, thereby disadvantaging the model. Even in this context, our model demonstrated competitive results compared to other methods, achieving the R^2 value and the mean absolute error (MAE) values of 0.924 and 4.12.

Table 1: Evaluation results on SuperCon data and comparison with other methods.

| | train dataset | MAE | R2 |
|------------------|----------------|-------------|--------------|
| Gu et al.[7] | SuperCon | - | 0.85 |
| Zhang et al.[4] | SuperCon | - | 0.929 |
| Stanev et al.[5] | SuperCon | - | 0.88 |
| Zeng et al.[9] | SuperCon | 4.21 | 0.97 |
| Dan et al.[8] | SuperCon | - | 0.907 |
| Ours | SuperCon + COD | 4.12 | 0.924 |

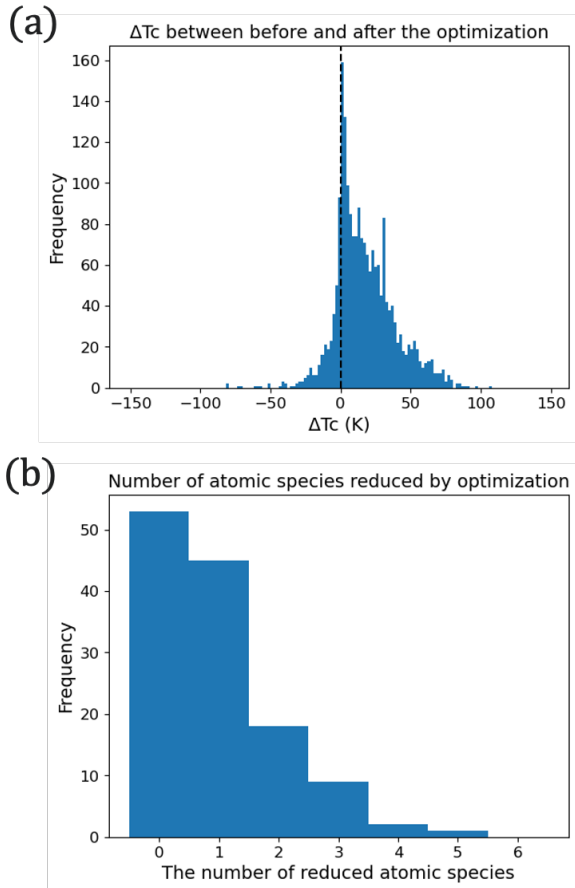


Figure 4: (a) Changes in Tc due to optimization. (b) Difference in number of element types before and after optimization (a positive number denotes the number of element type decreases after optimization).

Next, we show optimization results without integer loss (stage 2), using 8,192 superconductors randomly selected from the training data as initial candidates \hat{x} . We optimized \hat{x} using Adam optimizer with a learning rate of 0.001 for 1,000 steps. Optimization led to changes in atomic types and increased Tc for many candidates (Fig. 4). For instance, $\text{Ca}_{0.119}\text{Sr}_{0.059}\text{Ba}_{0.119}\text{Cu}_{0.179}\text{Hg}_{0.044}\text{O}_{0.477}$ (Tc: 104.3) was optimized to

$\text{Ca}_{0.227}\text{Sr}_{0.101}\text{Ba}_{0.054}\text{Cu}_{0.096}\text{Hg}_{0.150}\text{O}_{0.370}(\text{Tc}:155.03)$.

Despite the optimization aimed at maximizing Tc, Fig. 4(a) shows that Tc decreases for some candidates. We consider that this occurred because of the presence of numerous local minima. We believe that suboptimal solutions with lower Tc ensnare some solution candidates. This speculation is consistent with our observation that increasing the learning rate enhances the likelihood of identifying solutions with higher Tc (refer to Supplementary Material S4 for details). Furthermore, Fig. 4(b) demonstrates that the variety of atomic species consistently diminishes, with no observed increase.

Next, we examined the effects of conversion to integer numbers through $L_{integer,\{N\}}$. Candidates optimized without integer loss in stage 2 underwent further optimization in stage 3 with Eq.10 using Adam optimizer with a learning rate of 0.001 for 1,000 steps. The hyperparameter α was set to zero at the initial step and then increased linearly to 100,000 at step 1000. They were then compared to results using a simple rounding method. Note that this optimization used L_{int}^N or $L_{int,ES}^N$ instead of $L_{integer,\{N\}}$. As a result, L_{int}^N and $L_{int,ES}^N$ were able to integerized composition ratio while stably minimizing the decrease in Tc, especially $L_{int,ES}^N$ (Table 2). Examples of integerization are shown in Fig. 5.

Table 2: The average and standard deviation of changes in Tc when the same 8192 composition candidates were converted to integers.

| N | rule-based | L_{int}^N | $L_{int,ES}^N$ |
|----|------------|-------------|----------------|
| 8 | -35.5±42.3 | -37.7±29.6 | -13.4±19.0 |
| 12 | -19.3±40.6 | -22.4±23.1 | -6.7±11.1 |
| 16 | -10.2±38.8 | -11.9±16.3 | -4.5±7.7 |
| 20 | -7.9±39.0 | -9.9±14.1 | -3.0±5.3 |
| 40 | -3.4±38.8 | -4.9±8.2 | -1.0±8.2 |

Examples

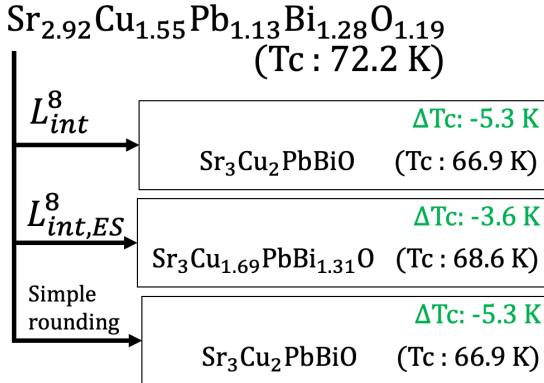


Figure 5: An example of $N=8$ for L_{int}^N and $L_{int,ES}^N$

Table 3: Hydride superconductor candidates discovered by GDMCD.

| Proposed materials | Tc (K) | Reference materials | Tc (K) |
|---------------------------------------|--------|---------------------|---------|
| Y_3H_{10} | 17.7 | YH_3 [32] | 40 |
| UH_8 | 7.1 | UH_7 [33] | 44 ~ 54 |
| TbNbH_2 | 53.4 | - | - |
| Cf_2H_{13} | 46.9 | - | - |
| Lr_3H_{17} | 48.4 | - | - |
| $\text{Lr}_7\text{Zn}_5\text{H}_{12}$ | 42.2 | - | - |

Next, we searched for new superconductors using GDMCD. We initialized and optimized solution candidates \hat{x} using a deep learning model f_{θ_x} to make Tc higher. We performed 1000 steps of optimization with Eq. 4, followed by 1000 steps of optimization with Eq. 10. We used the Adam optimizer with a learning rate of 0.01. We set $\{N\} = \{4, 5, \dots, 24\}$ for $L_{integer,\{N\}}$ and 300 (K) for y_t . We initialized 11,640 \hat{x}_t using two methods: directly utilizing randomly selected training data with Tc above 20 K and employing linear interpolation between two randomly selected training data points with Tc above 20 K, using an interpolation ratio sampled from the Beta distribution $B(10, 10)$. Parts of the optimization results are shown in Table 4 and 5. Table 4 lists the superconductor candidates discovered by GDMCD with element combinations identical to those in the training data. As demonstrated in Table 4, GDMCD could adjust existing compositions to make Tc higher. Furthermore, GDMCD was able to discover candidates with combinations of elements not present in the training dataset (Table 5). GDMCD not only rediscovered superconductors existing in the SuperCon validation or evaluation datasets but also identified candidates for novel superconductors not present in SuperCon.

Lastly, we employed a constraint to search for new hydride superconductors (HSC). We utilized the conditional vector $x_c = [0.5, 0, 0, \dots]$. For details, see supplementary material S5. Table 3 shows results. We found Y_3H_{10} (Tc: 17.7 K) and UH_8 (Tc: 7.1 K), where similar materials are validated or predicted as HSCs [33, 32] but not in the SuperCon dataset. We also discovered several undiscovered HSC candidates.

In summary, we introduced the GDMCD, an optimization-based approach for designing material compositions, and searched for high-Tc superconductors. This technique enables efficient searches beyond existing databases, facilitating the integerization of compositions and the element substitution. Additionally, it can adaptively impose constraints on inputs. By utilizing this, we could rediscover known hydrogen compound superconductors not listed in the database.

Although this method does not account for the prediction error of Tc in proposed materials, confirming Tc values through experimental or computational means remains crucial for these materials. Despite challenges, such as a

Table 4: Superconductor candidates discovered by GDMCD, whose combinations of elements are also found in the training data.

| Proposed materials | Tc (K) | Reference materials in SuperCon | Tc (K) | ΔT (K) |
|--|--------|--|--------|----------------|
| $\text{Ca}_{3.60}\text{Sr}_{9.40}\text{Bi}_6$ | 136.9 | CaSrBi | 109.0 | 26.9 |
| $\text{Ba}_5\text{Y}_3\text{Pr}_4\text{Cu}_9$ | 129.3 | $\text{Ba}_{0.9}\text{Y}_3\text{Pr}_2\text{Cu}_{0.1}$ | 85.1 | 44.2 |
| $\text{Ca}_2\text{SrFe}_2\text{Cu}_5\text{Bi}_3\text{O}_7$ | 128.0 | $\text{Ca}_2\text{Sr}_8\text{Fe}_{1.99}\text{CuBi}_2\text{O}_{0.01}$ | 74.1 | 53.9 |
| $\text{Ca}_2\text{Ba}_3\text{YCu}_3$ | 125.3 | $\text{Ca}_{0.1}\text{Ba}_{0.9}\text{Y}_3\text{Cu}_2$ | 85.2 | 40.1 |
| $\text{Ba}_2\text{Tm}_4\text{Cu}_5\text{O}_8$ | 117.6 | $\text{BaTmCu}_2\text{O}_3$ | 92.0 | 25.6 |
| $\text{Sr}_6\text{Cu}_3\text{Pb}_5\text{Bi}_2$ | 113.0 | $\text{SrCu}_{2.05}\text{Pb}_{1.9}\text{Bi}_{2.05}$ | 10.5 | 102.5 |
| $\text{Ba}_{0.4734}\text{Y}_4\text{Fe}_{1.5266}\text{Cu}$ | 104.7 | $\text{BaY}_{0.2}\text{Fe}_{2.8}\text{Cu}_2$ | 57.0 | 47.7 |
| $\text{LaCu}_3\text{Bi}_2\text{O}_9$ | 76.2 | $\text{LaCu}_{0.05}\text{Bi}_{1.95}\text{O}_{4.06}$ | 34.9 | 41.3 |
| $\text{Gd}_4\text{Fe}_5\text{As}_4\text{O}_4$ | 63.7 | $\text{GdFeAsO}_{0.7}$ | 53.6 | 10.1 |
| Mg_9Al_4 | 38.6 | $\text{Mg}_{0.18}\text{Al}_{0.28}$ | 1.6 | 38.0 |

Table 5: Superconductor candidates discovered by GDMCD, whose combinations of elements are **not** found in the training data.

| listed in SuperCon | Proposed materials | Tc (K) | Reference materials in SuperCon | Tc (K) |
|--------------------|---|--------|---|--------|
| Yes | $\text{Ba}_2\text{Y}_3\text{Er}_2\text{Cu}_4\text{O}_9$ | 77.6 | $\text{Ba}_{0.5}\text{Y}_7\text{Er}_2\text{Cu}_{0.5}\text{O}_3$ | 91.8 |
| Yes | $\text{Sr}_6\text{Y}_3\text{Mo}_4\text{WCu}_5$ | 38.4 | $\text{Sr}_{2.8}\text{Y}_{0.1}\text{Mo}_2\text{W}_{0.1}\text{Cu}$ | 40.5 |
| Yes | $\text{CaCu}_6\text{Zn}_7\text{Bi}_8$ | 20.3 | $\text{Ca}_2\text{Cu}_2\text{Zn}_3\text{Bi}_{0.005}$ | 94.0 |
| No | $\text{CaSr}_{10}\text{BaBiC}_5$ | 162.6 | - | - |
| No | $\text{Ca}_2\text{Cu}_2\text{Hg}_4\text{Pb}_6\text{O}_6$ | 140.2 | - | - |
| No | $\text{Mg}_3\text{Ca}_3\text{Ba}_2\text{Cu}_4\text{Tl}_6$ | 131.7 | - | - |
| No | $\text{LiCa}_3\text{Sr}_5\text{Ba}_{20}\text{Bi}_8$ | 127.4 | - | - |
| No | $\text{Sr}_2\text{V}_8\text{Cu}_3\text{Hg}_2$ | 125.7 | - | - |
| No | $\text{SrCu}_2\text{Tl}_{11.0}\text{O}_{3.0}$ | 120.9 | - | - |
| No | $\text{CaBa}_4\text{Fe}_5\text{Tl}_9$ | 97.4 | - | - |
| No | $\text{Ba}_{2.09}\text{Y}_{1.91}$ | 31.1 | - | - |

small dataset and missing critical information like pressure—crucial for hydride superconductors—the MAE of 4.12 reflects a reasonable accuracy in the predicted Tc values of the proposed materials. This research underscores the potential of gradient-based methods in atomic-scale

material design. Our method is versatile and applicable to other fields beyond superconductors. In future work, we will engage in optimizing not only the composition but also the crystal structure to achieve the desired properties.

References

- [1] Fujii, A., Tsunashima, H., Fukuhara, Y., Shimizu, K., and Watanabe, S. (2023). arXiv preprint arXiv:2304.13860.
- [2] Ren, S., Mahendra, A., Khatib, O., Deng, Y., Padilla, W. J., and Malof, J. M. (2022). *Nanoscale*, 14(10), 3958-3969.
- [3] Konno, T., Kurokawa, H., Nabeshima, F., Sakishita, Y., Ogawa, R., Hosako, I., and Maeda, A. (2021). *Physical Review B*, 103(1), 014509.
- [4] Zhang, J., Zhu, Z., Xiang, X.D., Zhang, K., Huang, S., Zhong, C., Qiu, H.J., Hu, K. and Lin, X. (2022). *The Journal of Physical Chemistry C*, 126(20), 8922-8927.
- [5] Stanev, V., Oses, C., Kusne, A. G., Rodriguez, E., Paglione, J., Curtarolo, S., and Takeuchi, I. (2018). *NPJ Computational Materials*, 4(1), 29.
- [6] Matsumoto, K., and Horide, T. (2019). *Applied Physics Express*, 12(7), 073003.
- [7] Gu, L., Liu, Y., Chen, P., Huang, H., Chen, N., Li, Y., ... and Su, Y. (2023). arXiv preprint arXiv:2308.11160.
- [8] Dan, Y., Dong, R., Cao, Z., Li, X., Niu, C., Li, S., and Hu, J. (2020). *IEEE Access*, 8, 57868-57878.
- [9] Zeng, S., Zhao, Y., Li, G., Wang, R., Wang, X., and Ni, J. (2019). *NPJ Computational Materials*, 5(1), 84.
- [10] Kingma, D. P., and Ba, J. (2014). arXiv preprint arXiv:1412.6980.
- [11] He, K., Zhang, X., Ren, S., and Sun, J. (2016). In *Proceedings of the IEEE conference on computer vision and pattern recognition* (pp. 770-778).

- [12] Zagoruyko, S., and Komodakis, N. (2016). arXiv preprint arXiv:1605.07146.
- [13] "MDR SuperCon Datasheet Ver.220808". . . , no. . . (2022): <https://doi.org/10.48505/nims.3837>
- [14] Vaitkus, A., Merkys, A., Sander, T., Quirós, M., Thiessen, P. A., Bolton, E. E. and Gražulis, S. (2023). *Journal of Cheminformatics*, 15.
- [15] Merkys, A., Vaitkus, A., Grybauskas, A., Konovalovas, A., Quirós, M. and Gražulis, S. (2023). *Journal of Cheminformatics*, 15.
- [16] Vaitkus, A., Merkys, A. and Gražulis, S. (2021). *Journal of Applied Crystallography*, 54(2), 661-672.
- [17] Quirós, M., Gražulis, S., Girdzijauskaitė, S., Merkys, A. and Vaitkus, A. (2018). *Journal of Cheminformatics*, 10.
- [18] Merkys, A., Vaitkus, A., Butkus, J., Okulič-Kazarinas, M., Kairys, V. and Gražulis, S. (2016). *Journal of Applied Crystallography*, 49(1), 292–301
- [19] Gražulis, S., Merkys, A., Vaitkus, A. and Okulič-Kazarinas, M. (2015). *Journal of Applied Crystallography*, 48(1), 85-91.
- [20] Gražulis, S., Daškevič, A., Merkys, A., Chateigner, D., Lutterotti, L., Quirós, M., Serebryanaya, N. R., Moeck, P., Downs, R. T. and LeBail, A. (2012). *Nucleic Acids Research*, 40, D420-D427.
- [21] Gražulis, S., Chateigner, D., Downs, R. T., Yokochi, A. T., Quirós, M., Lutterotti, L., Manakova, E., Butkus, J., Moeck, P. and Le Bail, A. (2009). *Journal of Applied Crystallography*, 42, 726-729.
- [22] Downs, R. T. and Hall-Wallace, M. (2003). *American Mineralogist*, 88, 247-250.
- [23] Sohn, K., Lee, H., and Yan, X. (2015). *Advances in neural information processing systems*, 28.
- [24] Mirza, M., and Osindero, S. (2014). arXiv preprint arXiv:1411.1784.
- [25] Ho, J., Jain, A., and Abbeel, P. (2020). *Advances in neural information processing systems*, 33, 6840-6851.
- [26] Zhong, C., Zhang, J., Lu, X., Zhang, K., Liu, J., Hu, K., ... and Lin, X. (2023). *ACS Applied Materials & Interfaces*.
- [27] Quinn, M. R., and McQueen, T. M. (2022). Identifying New Classes of High Temperature Superconductors With Convolutional Neural Networks. *Frontiers in Electronic Materials*, 2, 893797.
- [28] Kim, E., and Dordevic, S. V. (2023). ScGAN: a generative adversarial network to predict hypothetical superconductors. *Journal of Physics: Condensed Matter*, 36(2), 025702.
- [29] Liu, Gang, Jiabin Xu, Tengfei Luo, and Meng Jiang. arXiv preprint arXiv:2401.13858 (2024).
- [30] Lai, Qingsi, Lin Yao, Zhifeng Gao, Siyuan Liu, Hongshuai Wang, Shuqi Lu, Di He, Liwei Wang, Cheng Wang, and Guolin Ke. arXiv preprint arXiv:2401.03862 (2024).
- [31] Zeni, C., Pinsler, R., Zügner, D., Fowler, A., Horton, M., Fu, X., ... and Xie, T. (2023). arXiv preprint arXiv:2312.03687.
- [32] Kim, D. Y., Scheicher, R. H., Mao, H. K., Kang, T. W., and Ahuja, R. (2010). *Proceedings of the National Academy of Sciences*, 107(7), 2793-2796.
- [33] Kruglov, I. A., Kvashnin, A. G., Goncharov, A. F., Oganov, A. R., Lobanov, S. S., Holtgrewe, N., ... and Yamilkin, A. V. (2018). *Science advances*, 4(10), eaat9776.
- [34] Hull, J. R. (2003). *Reports on Progress in Physics*, 66(11), 1865.

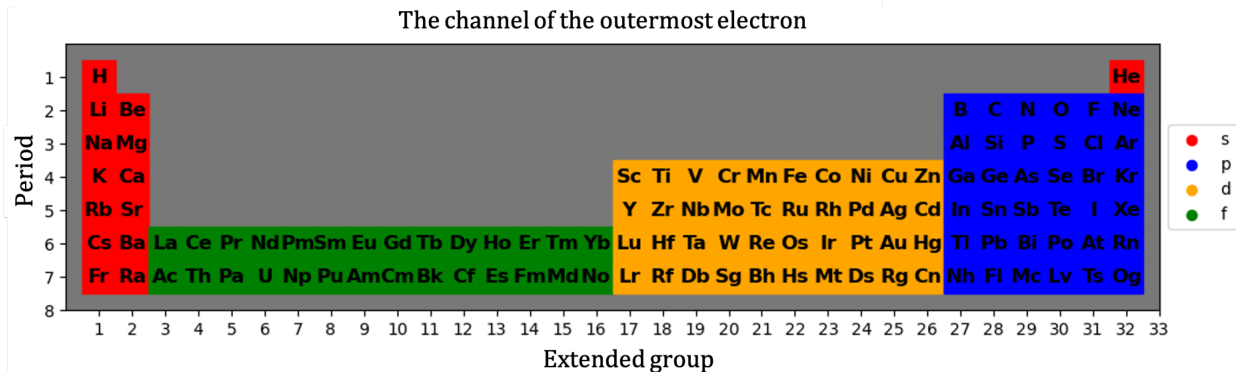


Figure 6: The corresponding channel of the outermost electron for each element.

A Supplementary Material

S1 Atomic representation

As atomic features a , we utilized flag representations for the s, p, d, and f electron orbitals as embedded in the periodic table[3]. Each atom has a feature tensor with dimensions of $4 \times 7 \times 32$, representing the channels for the s, p, d, and f electron orbitals, periods, and groups. Note that, due to the extension of lanthanides and actinides in the group direction, the third dimension (group) extends to 32, not 18. For any atom i , its feature a^i assigns a value of 1 at the position in the periodic table corresponding to the outermost electron's channel and 0 values for all other positions.

$$a \in \{0, 1\}^{118 \times 4 \times 7 \times 32} \quad \sum_{j,k,l} a^i = 1 \quad (14)$$

$$a_{jkl}^i = \begin{cases} 1 & \text{if atom } i \text{ has its outermost electrons, family (group),} \\ & \text{and period corresponding to } j, k, \text{ and } l. \\ 0 & \text{otherwise} \end{cases} \quad (15)$$

For instance, the hydrogen atom, which has a 1s electron in its outermost shell and belongs to the first period and group, is represented by the feature \mathbf{a}^{H} . This feature has a value of one at position (1, 1, 1) and zeroes elsewhere. Similarly, the feature for chlorine, \mathbf{a}^{Cl} , which contains 3p electrons in its outer shell and is located in the third period and seventeenth group, has a value of 1 at position (2, 3, 31) and zeroes elsewhere. Fig 6 illustrates the corresponding channel of the outermost electron for each element. The composition's representation is calculated by computing the product of the distribution vector x and the atomic features a , as shown in Fig 7.

S2 Dataset

We used the SuperCon dataset for superconductor materials. For preprocessing, we excluded substances whose compositions were not quantitatively specified, such as those denoted by variables (e.g., x, y, z). We also used the Crystallography Open Database (COD) for the non-superconductor materials. Furthermore, compositions identical to those in the SuperCon data were excluded from the COD data.

For both SuperCon and COD, compositions were represented by 118-dimensional (from H to Og) distribution vectors x , normalized to sum to 1. The critical temperature (T_c) was used as the target variable y , setting $y=0$ for non-superconducting materials from the COD dataset and using the actual T_c values from the SuperCon dataset. For substances with identical compositional ratios but have different T_c values, we calculated the mean T_c value for use. Consequently, we obtained 16,550 data points for the SuperCon dataset and 52,787 data points for the COD dataset. We then randomly split these into training, validation, and test sets in the ratios of 0.80:0.05:0.15, respectively.

However, we were concerned about the model's accuracy due to the lower number of superconductors compared to non-superconductors in the training data. Therefore, to address this imbalance, we augmented the training data

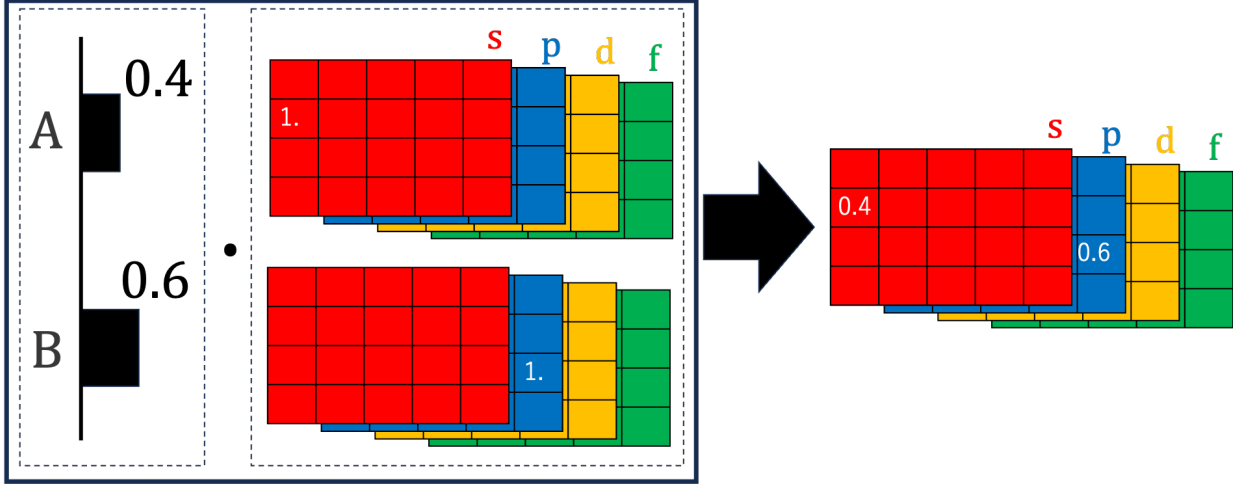


Figure 7: The representation of the composition A_2B_3

by tripling the number of instances from the SuperCon dataset through replication. As a result, the training dataset expanded to 78,877 data points, with the augmented SuperCon data contributing 38,232 (12,744 original data points tripled). Note that we did not augment the validation and test datasets, resulting in 2,565 validation data points (612 from SuperCon) and 13,381 test data points (3,194 from SuperCon).

S3 Reducing false positives

Here, we address the issue of false positives, that is, the incorrect prediction of non-superconductors as superconductors. Konno et al.[3] say that models trained exclusively on the SuperCon dataset tend to produce a significant number of false positives, although this claim has not been numerically validated. Hence, we numerically assessed how incorporating the COD dataset, which consists of non-superconductors, impacts the rate of false positives.

We performed this assessment using our model, a ResNet18 regression model and adopted the precision score as our metric. The precision score is defined as $tp/(tp + fp)$, where tp (true positive) denotes the probability of accurately predicting a superconductor ($y>0$) as superconductor (i.e., $f_{\theta_*}(x) > 0$), and fp (false positive) represents the probability of mistakenly predicting a non-superconductor ($y=0$) as a superconductor (i.e., $f_{\theta_*}(x) > 0$).

Table 6 provides a comparison of precision scores between models trained on the SuperCon dataset alone and those trained on both SuperCon and COD datasets. It is evident that models trained with the inclusion of the COD dataset exhibit a significantly higher precision score compared to those trained exclusively on the SuperCon dataset. This outcome underscores the necessity of integrating non-superconductors into the training process for superconductor material design tasks, where non-superconductors might emerge as potential candidates.

S4 The effect of change on the learning rate

We investigated the impact of altering the learning rate on optimization with Equation 4, employing the same 2048 initial solution candidates. Increasing the learning rate enhances the likelihood of identifying solutions with higher T_c , though it lowers T_c for some cases (Table 7).

Table 6: Comparison of the precision scores between models trained on the SuperCon dataset and those trained on SuperCon+COD.

| Training data | Precision score |
|---------------|-----------------|
| SuperCon | 0.065 |
| SuperCon+COD | 0.804 |

Table 7: Statistics on the change in T_c , denoted as ΔT , before and after the optimization process with learning rates set at 0.01 and 0.0001. This table displays the ΔT values of 2048 solution candidates at the 0.0 (minimum), 0.25, 0.5 (median), 0.75, and 1.0 (maximum) percentiles.

| percentile | $\Delta T@lr=0.01$ (K) | $\Delta T@lr=0.0001$ (K) |
|------------|------------------------|--------------------------|
| 0.00 | -133.90 | -81.22 |
| 0.25 | 0.36 | 2.57 |
| 0.50 | 15.81 | 13.64 |
| 0.75 | 35.50 | 30.01 |
| 1.00 | 123.39 | 107.65 |

Table 8: MAE scores for predicting the superconductor T_c in the test data. Note that the test datasets for D_{HSC1} and D_{HSC200} are the same, but that of D_{random} is not.

| Training data | The proportion of HSCs in the training data | MAE |
|---------------|---|------|
| D_{random} | 0.049% | 4.12 |
| D_{HSC1} | 0.051% | 4.24 |
| D_{HSC200} | 50.263% | 4.11 |

S5 Searching for new hydride superconductors

Hydride superconductors (HSCs) represent a mere 0.05% of the SuperCon dataset, having been discovered recently. To enhance the detection accuracy of HSC, we created the dataset D_{HSC1} , incorporating all HSCs into the training data. Furthermore, the number of HSCs is extremely limited. The count differs across compositional combinations (for example, there are over ten compositions for H_xPd_{1-x} but only a single type of H_xLa_{1-x}). Consequently, after balancing the counts for each compositional combination through replication, we developed the dataset D_{HSC200} , which was expanded by a factor of 200. As a result, HSCs comprised 50.3% of the total training data. We evaluated the ResNet18 regression model trained with these datasets based on MAE and found that no decline in the MAE score of other superconductors (Table 8).

We trained a wide-ResNet101-2[12] regression model with D_{HSC200} , with a learning rate of 0.00001, batch size 256, and the Adam optimizer for 250 epochs, denoted f_{HSC,θ_*} . Several HSCs of binary systems have been identified to date, wherein hydrogen accounts for over 50% of their composition ratios. Hence, employing the constraint that hydrogen comprises over 50% of compositions, we search for HSCs of binary or ternary systems. Specifically, we employed the constraint $x_c = [0.5, 0.0, \dots]$. For searching binary systems, \hat{x}_{opt} is initialized in the following:

$$\hat{x}_{opt}^i = \begin{cases} \frac{n-1}{n} - 0.5 & (i \text{ is hydrogen}) \\ 1 - \frac{n-1}{n} & (i \text{ is Atom a}) \\ 0 & (\text{else}) \end{cases} \quad (16)$$

Here, $n = 2, 3, 4, \dots, 10$. In the case of ternary systems, \hat{x}_{opt} is initialized in the following:

$$\hat{x}_{opt}^i = \begin{cases} 0.25 & (i \text{ is Atom a or b}) \\ 0 & (\text{else}) \end{cases} \quad (17)$$

We used a total of 14,580 \hat{x}_{opt} across combinations of Atom a and n in all binary systems excluding hydrogen (117×8) and combinations of Atom a and b in ternary systems (117×116). Solution candidates \hat{x} are represented in the following:

$$\hat{x} = \hat{x}_{opt} + x_c \quad s.t. \quad \sum_{i=1}^{118} \hat{x}_{opt}^i = 0.5, \quad 0 \leq \hat{x}_{opt}^i \leq 0.5 \quad (18)$$

Then, we performed 500 steps of optimization with Eq. 4, followed by 500 steps of optimization with Eq. 10 using f_{HSC,θ_*} . We used the Adam optimizer with a learning rate of 0.01. We set $\{N\} = 4, 5, \dots, 24$ for $L_{integer,\{N\}}$ and 300 (K) for y_t .